Impact of *df/dt* Inertia Control on Doubly Fed Induction Generator Type Wind Turbine

Hua Huang[1], *Xin* Tao[2], *Xu* Tian[2], *and Fei* Peng[2]

[1]Huazhong University of Science and Technology, 430074, Wuhan, China
[2]State Grid Qinghai Electric Power Company, Xining 810000, Qinghai Province, China

Abstract. the supplemental *df/dt* control is the common method for wind power generation to support system inertial response. This paper investigates the impact of the *df/dt* inertia controller on doubly fed induction generator (DFIG) type wind turbine. The controller is usually a high pass filter. Two parameters which are the gain and the time constant are considered. By constructing the linearized model of DFIG, the impacts of the two parameters of the controller are discussed. It shows that with different phase locked loop (PLL) parameters and current control parameters, different time constants and gains are required to ensure the DFIG stability. The time domain simulation validates the result.

1 Introduction

As more and more wind power generation injecting to power system, the lack of inertia becomes significant. The solution is to make the wind power generation support inertial response. The common method is to detect the change rate of grid frequency (*df*/*dt*) to make wind power generators generate extra active power [1-7]. This control imitates the rotor dynamic process of synchronous generator (SG). The gain between *df*/*dt* and the extra active power is considered as the inertia constant from wind power generation [5]. Since it is difficult to implement the derivative control, a high pass filter is often used. Due to the simple physical significance and control logic, it is expected to widely use in more and more wind power generators.

Obviously, the dynamic properties of wind power generator in electromechanical time scale are changed due to the supplemental inertia control. Researches naturally focus on the response of wind power generator and its impact on power system stability in electromechanical time scale. For example, in [3], the impact of different parameters of the *df*/*dt* controller was studied, and it concluded that the high pass filter time constant will reduce the effect of the inertial response. In [8-9], the impact of doubly fed induction generator (DFIG) inertia control on SG's small signal stability was studied.

The researches are based on the condition that the wind power generations are stable when applied the supplemental control. However, in some situations, improper setting *df/dt* controller parameters will lead to instability. Few researches have focused on the influence of the *df/dt* control on wind power generator itself. In [10], it mentioned that the *df/dt* control will deteriorate the DFIG shafting dynamic. However, the detailed analysis is not given.

In this paper, we focus on the impact of the supplemental *df/dt* control on DFIG's electromagnetic dynamics. By analyzing the linearized model of DFIG in electromagnetic time scale, it is found the *df/dt* control will influence the stability of the DFIG's rotor side current control. The smaller time constant and larger gain of the *df/dt* controller tends to lead to instability. The analysis reveals that different phase locked loop (PLL) parameters and current control parameters will require different time constant and gain to ensure the DFIG stable.

The rest of the paper is recognized as follows: section II describes the control and establishes the linearized electromagnetic model. Section III analyzes the stability of *df/dt* on DFIG current control with consideration of different impact factors. Section IV gives the simulation results. The conclusion is in section V.

2 Control strategy and modelling of DFIG

2.1 Control Strategy of DFIG

The control strategy of a DFIG is shown in Fig. 1 [11]. The maximum power point tracking (MPPT) algorithm generates the desired rotor speed, and the rotor speed controller generates electromagnetic torque reference. The output of *df/dt* controller, as shown in the red block in Fig. 1, is added to the torque reference to compose the final electromagnetic torque reference. As the stator voltage is approximately equal to 1 in per unit, the value of electromagnetic torque is approximately equal to the active power component of rotor side current. For

simplicity, the d-axis rotor current reference, which represents the active power component, is equal to the final electromagnetic torque reference. The frequency detection is come from the phase locked loop (PLL). The grid side control is in normal control mode and for simplicity is not plotted in Fig. 1.

The rotor side current control adopts the common vector control strategy. It is also shown in Fig. 1.

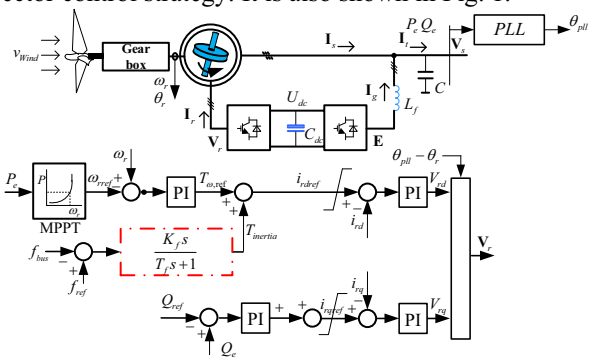

Fig. 1. DFIG rotor side control with df/dt inertia control.

2.2 Model of DFIG Rotor Side Current Control with Inertia Control

The analyzed system is shown in Fig. 2 that a single equivalent DFIG connects to an infinite bus through a long transmission line. As the outer speed control loop and reactive power control loop are relatively slow, when considering the rotor side current control, its influence can be neglected. Hence, the d-axis current reference is only changed by the *df/dt* control, while the q-axis current reference is unchanged.

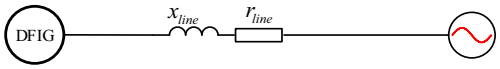

Fig. 2. Single DFIG connects to a infinite bus through transmission lines.

2.2.1 Electric Circuit Modeling

Define the stator current injecting to grid is the stator current positive direction, and the rotor current injecting to rotor is the rotor current positive direction. Hence, the stator voltage vector $\mathbf{V}_s$ and rotor voltage vector $\mathbf{V}_r$ can be expressed as:

$$\begin{aligned}\mathbf{V}_s + R_s\mathbf{I}_s + j\omega_1 L_s\mathbf{I}_s + dL_s\mathbf{I}_s/dt = dL_m\mathbf{I}_r/dt + j\omega_1 L_m\mathbf{I}_r \\ \mathbf{V}_r - R_r\mathbf{I}_r + j\omega_{slip} L_m\mathbf{I}_s + dL_m\mathbf{I}_s/dt = dL_r\mathbf{I}_r/dt + j\omega_{slip} L_r\mathbf{I}_r\end{aligned} \quad (1)$$

Where $\mathbf{I}_s$ and $\mathbf{I}_r$ are stator current and rotor current vector. L_s is the stator inductor, L_r is the rotor inductor, L_m is the mutual inductor, R_s is the stator resistor, and R_r is the rotor resistor. For simplicity, the grid side converter current injection is ignored as the mainly characteristics are reflected in rotor side converter. However, the capacitor is considered as it significantly affects the stability. According to the grid circuit, the stator voltage can be also expressed as:

$$\mathbf{V}_s = \mathbf{V}_b + R_l\mathbf{I}_{s1} + j\omega_1 L_l\mathbf{I}_{s1} + dL_l\mathbf{I}_{s1}/dt \quad (2)$$

$$j\omega_1 C(\mathbf{V}_s - \mathbf{I}_{s2}R_c) + dC(\mathbf{V}_s - \mathbf{I}_{s2}R_c)/dt = \mathbf{I}_{s1} \quad (3)$$

$$\mathbf{I}_s = \mathbf{I}_{s1} + \mathbf{I}_{s1} \quad (4)$$

Where $\mathbf{V}_b$ is the voltage of the infinite bus. $\mathbf{I}_{s1}$ and $\mathbf{I}_{s2}$ are the current in line and in capacitor respectively. C is the capacitor and R_c is the resistor on it. The equations are all in a public constant speed rotating reference. Let the *d*-axis of the public constant speed rotating reference overlaps with the stator voltage vector in steady state. Eliminate the stator current and ignore the rotor speed variation, in small signal equation, by replacing the differential operation by Laplace operator *s*, the rotor current and stator voltage can be expressed as in Eq. (5), the expression can be seen in Appendix.

$$\begin{aligned}\Delta\mathbf{V}_s &= \mathbf{G}_{VV}(s)\Delta\mathbf{V}_r \\ \Delta\mathbf{I}_r &= \mathbf{G}_{VI}(s)\Delta\mathbf{V}_r\end{aligned} \quad (5)$$

2.2.2Control System Modeling

In the control system, the variables are in PLL reference frame. In steady state, the d-axis of the public constant speed rotating reference overlaps with the d-axis of PLL. However, in dynamic process, they are inconsistent. The relation can be seen in Fig. 3.

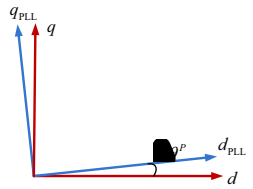

Fig. 3. The axis relation.

Hence, according to the phase relation shown in Fig. 3, we can get:

$$\begin{aligned}i_{rd}^p &= i_{rd}\cos\Delta\theta^p + i_{rq}\sin\Delta\theta^p \\ i_{rq}^p &= i_{rq}\cos\Delta\theta^p - i_{rd}\sin\Delta\theta^p\end{aligned} \quad (6)$$

Where the superscript P means the variables are in PLL reference frame. θ^P is the output phase angle of PLL. Then the linear small disturbance equation of rotor current can be expressed as:

$$\begin{aligned}\Delta i_{rd}^p &= \Delta i_{rd} + i_{rq0}\Delta\theta^p \\ \Delta i_{rq}^p &= \Delta i_{rq} - i_{rd0}\Delta\theta^p\end{aligned} \quad (7)$$

The subscript 0 means initial value. With the same process, we can get the linear small disturbance equation of the rotor voltage in public constant speed rotating reference expressed as:

$$\begin{aligned}\Delta V_{rd} &= \Delta V_{rd}^p - V_{rq0}\Delta\theta^p \\ \Delta V_{rq} &= \Delta V_{rq}^p + V_{rd0}\Delta\theta^p\end{aligned} \quad (8)$$

$\Delta\theta^P$ is come from PLL. The equivalent construction of PLL is shown in Fig. 4, where the input is the stator voltage phase θ_{grid}, and the output is θ^P.

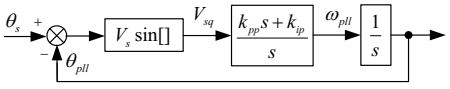

Fig. 4. Diagram of PLL.

Considering that the stator voltage magnitude in per unit is approximately equal to 1, and in steady state, θ_{grid}, is equal to θ^P, from Fig. 4, we can get the linear small disturbance equation of $\Delta\theta^P$ is expressed as:

$$\Delta\theta^p \approx \frac{k_{pp}s+k_{ip}}{s^2+k_{pp}s+k_{ip}}\Delta\theta_{grid} = G_{pll}(s)\Delta\theta_{grid} \quad (9)$$

In the public constant speed rotating reference, the stator voltage phase angle variation can be expressed as:

$$\Delta\theta_{grid} \approx \Delta V_{sq}/V_{s0} = \Delta V_{sq}/V_{sd0} \quad (10)$$

A reality should also be paid attention is the control delay effect. It is caused by the digital control. To simplify the analysis, the sampling time delay and output time delay are unified modeled that is replaced by a unit time delay. To linearize the discrete unit time delay, the Pade equivalent method is adopted. Synthetically considering the simplicity and accuracy, the second order Pade equivalent is adopted as shown in (11).

$$\frac{1}{z} \approx G_d(s) = \frac{1-\frac{T_d}{2}s+\frac{T_d^2}{12}s^2}{1+\frac{T_d}{2}s+\frac{T_d^2}{12}s^2} \quad (11)$$

Where T_d=1.5T_s, and T_s is the sampling time. Hence, the rotor side current control linear small disturbance block diagram can be plotted in Fig. 5.

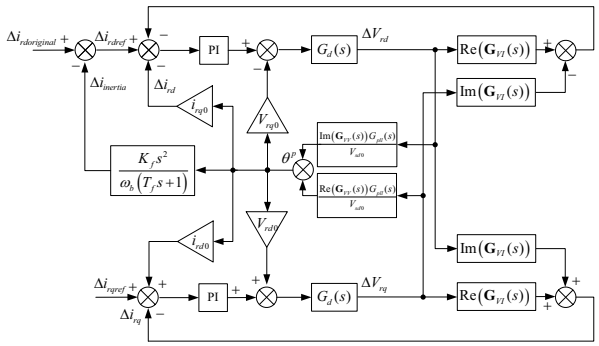

Fig. 5. Small signal analysis diagram of DFIG rotor current control loop.

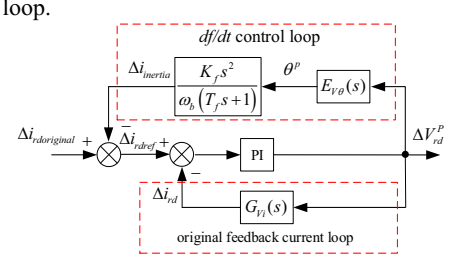

Fig. 6. Small signal diagram of DFIG *d*-axis rotor current control.

3 Stability Analysis

The *df/dt* control is added at d-axis rotor current control loop, so the study object should focus on the *d*-axis current control loop. In order to understand the impact of the *df/dt* control, according to Fig. 5, we separate the analysis loop into two parts as shown in Fig. 6. The first part named as original feedback current loop represents the normal current control process. The other part named *df/dt* control loop represents the supplemental impact introduced by the *df/dt* control. The following study is based on Fig. 6.

3.1 Impact of *df/dt* parameters

In Fig. 6, the *df/dt* control loop can be seen as an external part of the feedback rotor current. The bode diagram of this external loop and the original feedback current loop is plotted in Fig. 7. We can see that, the *df/dt* control's property is similar with the original feedback current loop, especially in phase properties. The main difference is the magnitude. Hence, after adding *df/dt* control, it equivalently increases the rotor current control loop's bandwidth.

In Fig. 7(a), the gain of the *df/dt* controller K_f is set to 10, and the time constant of the *df/dt* controller T_f is set to 0.1, 0.5, 1 separately. The dotted line represents the original current feedback loop. It shows that with the time constant of the *df/dt* controller decreasing, the magnitude of the *df/dt* control loop increases. Hence, according to the classical linear control theory, the bode diagram of the total open loop of the current control shows that with the time constant of the *df/dt* controller decreasing, the system tends to be unstable.

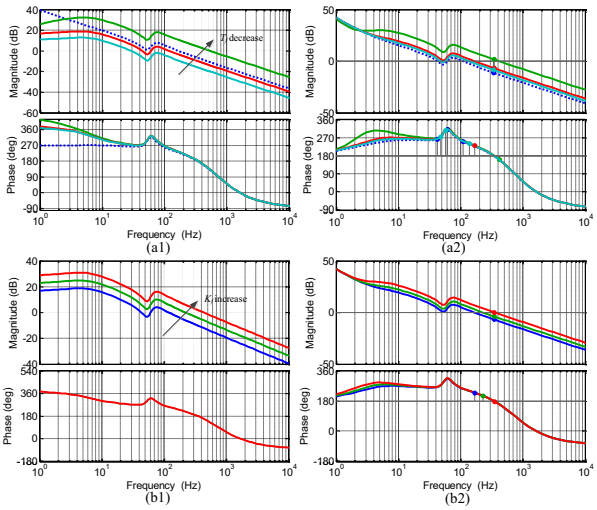

Fig. 7. Bode diagram of df/dt control loop and original feedback current loop.

In Fig. 7(b), the time constant of the *df/dt* controller T_f is set to 0.5, and the gain of the *df/dt* controller is K_f set to 10, 20, 40 separately.it shows that with the gain of the *df/dt* controller increasing, the *magnitude* of the *df/dt* control loop increases. Hence, the bode diagram of the total open loop of the current control shows that with the gain of the *df/dt* controller decreasing, the system tends to be unstable.

3.2 Impact of PLL parameters

The frequency detection is from PLL. So the transfer function of PLL will also influence the dynamic of *df/dt* control loop. Meanwhile, the original feedback current loop is also influenced by PLL.

The bode diagrams with different PLL parameters are plotted in Fig. 8. The dotted lines represent the original feedback current loop. In Fig. 8(a), it can be seen that the with different PLL parameters, the original feedback current loop almost remains unchanged. However, the magnitude of the *df/dt* control loop will be larger when the PLL parameters are larger. Consequently, in Fig. 8(b), the phase margin of the open loop of the current control become smaller, with PLL parameters become larger, the system tends to be unstable.

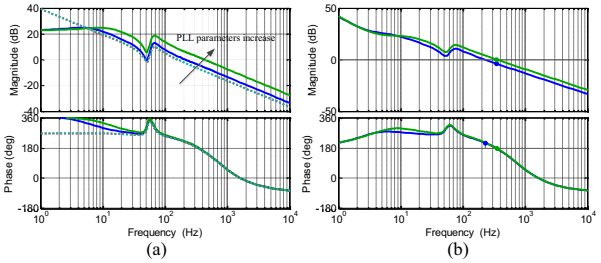

Fig. 8. Bode diagram with different PLL parameters.

3.3 Impact of Current controller parameters

The open loop gain of the rotor current control is also depended on the current controller. Meanwhile, the current control parameters will also influence the *df/dt* control loop and the original feedback current loop.

Fig. 9 shows the bode diagrams with different current control parameters. The dotted lines represent the original feedback current loop. In Fig. 9(a), it can be seen that with different current control parameters, the original feedback current loop and the *df/dt* control loop are almost unchanged. Hence, it the larger current control parameters will directly increase the gain of the current control's open loop. The stability tends to decrease.

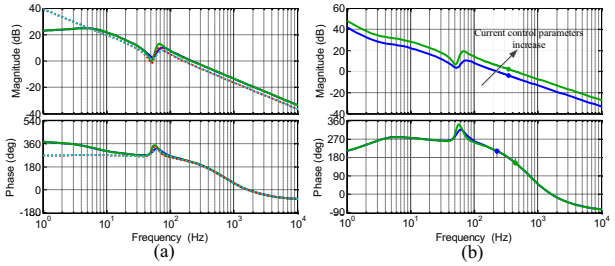

Fig. 9. Bode diagram with different current control parameters.

4 Time Domain Simulation Results

Table I. DFIG parameters for basic case

Items	value
Grid impedance and resistor	6.6858e-04H, 0.042Ω
df/dt controller	K_f=20, T_f=0.5
k_p and k_i of PLL	60, 1400
k_p and k_i of current controller	0.6, 8

The time domain simulation is carried out in MATLAB/SIMULINK. The simulation step size is 5e-6s to guarantee the discrete simulation will not affect the stability phenomena. The switching frequency of the DFIG control system is 2000Hz.

A basic case is used to compare the different impact factors. In this basic case, the core parameters are shown in Table I. Other parameters are shown in Appendix.

Different factors are compared in time simulations. The *d*-axis rotor current in control system and stator current are plotted. At t=5s, the *df/dt* control is added.

In Fig. 10, the result of different *df/dt* control parameters are shown. Fig. 10(a) is the basic case. In Fig. 10(b), the K_f is 40 and T_f is 0.5. In Fig. 10(b), the K_f is 20 and T_f is 0.1. In the basic case, it is stable. When increase the gain K_f, the system become unstable, the oscillation in i_{rd} gradually divergence. When reduce the time constant T_f, it can also lead to the system unstable. The results fit the analyzed above. The stator current shows the stable waveform and the unstable waveform. When it becomes unstable, the waveform become obviously distortion.

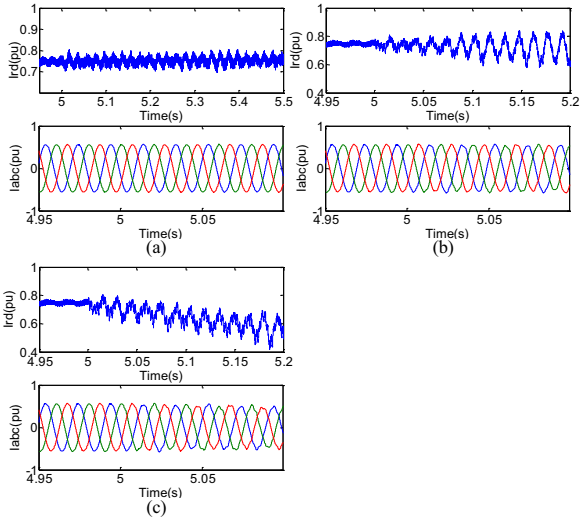

Fig.10. DFIG d-axis rotor current in control system and stator current with different df/dt controller parameters.

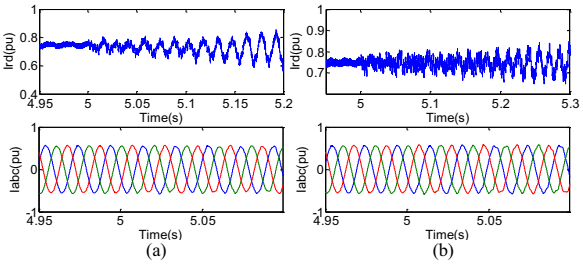

Fig. 11. DFIG d-axis rotor current in control system and stator current (a) different PLL parameters; (b) different current control parameters.

In Fig. 11(a), the different PLL parameters are compared. In this case, the k_p and k_i of PLL are tuned to 120 and 6400. Compared to the basic case, the larger PLL parameters tends to lead to unstable. The

phenomenon is similar that the oscillation gradually divergence.

In Fig. 11(b), the different current control parameters are compared. In this case, the k_p *and* k_i of current controller are tuned to 1.2 and 16. As analyzed above, with the gain of the current controller increase, the stability becomes worsen.

The four comparisons very well fits the analyzed conclusions before.

5 Conclusions

The classical *df/dt* control in some circumstances will leads to undesired instability issues in DFIG current control. In this paper, the reason why it will bring instability is analyzed, and the impact factors including grid strength, PLL parameters and current controller parameters are considered. The results show that the gain and time constant of *df/dt* controller cannot be arbitrary set. When the PLL parameters are large, and current controller parameters are large, the gain of *df/dt* should be smaller and the time constant of *df/dt* should be larger to guarantee the stability. The time domain simulation validates the results. The results of the paper are desired to offer a limitation for setting the *df/dt* controllers.

Acknowledgments:

The work presented in this paper was fully supported by the grant from Basic Research Project of Qinghai Province of China (2016-ZJ-767), and State Grid Corporation Science and Technology Project (52283015000M).

APPENDIX

Table II. DFIG parameters

Symbol	Description	value
R_s	Stator resistance	0.023 p.u.
R_r	Rotor resistance	0.016 p.u.
L_s	Stator self-inductance	3.08 p.u.
L_r	Rotor self-inductance	3.06 p.u.
L_m	Mutual inductance	2.9 p.u.
P_N	Rated power	1.0MW
U_N	Rated stator voltage	690 V
U_{rn}	Rated open loop rotor voltage	1950V
f_N	Rated frequency	50 Hz

References

1. J. Ekanayake and N. Jenkins, "Comparison of the response of doubly fed and fixed-speed induction generator wind turbines to changes in network frequency," IEEE Trans. Energy Conversion, vol. **19**, no. 4, pp. 800-802, Dec. 2004.
2. J. Morren, S. W. H. de Haan, W. L. Kling, and J. A. Ferreira, "Wind turbines emulating inertia and supporting primary frequency control, " IEEE Trans. Power Systems, vol. **21**,no. 1, pp. 433-434, Feb. 2006.
3. M. Kayikçi and J. V. Milanovic´, "Dynamic contribution of DFIG-based wind plants to system frequency disturbances," IEEE Trans. Power Systems, vol. **24**, no. 2, pp.859-867, May. 2009.
4. G. Ramtharan, J. B. Ekanayake and N. Jenkins, "Frequency support from doubly fed induction generator wind turbines" IET Renewable Power Generation, vol. **1**, no. 1, pp. 3–9, Mar. 2007.
5. J. Mauricio, A. Marano, A. Expósito, and J. Ramos. "Frequency regulation contribution through variable speed wind energy conversion systems", IEEE Trans. Power Systems., vol. **24**, no. 1, pp. 173-180, Feb. 2009
6. N. W. Miller, K. Clark, M. E. Cardinal, R. W. Delmerico "GE wind plant dynamic performance for grid and wind events" AEE TECH WIND GRID, Apr. 2009.
7. N.W. Miller, K. Clark, M. Shao, "Frequency responsive wind plant Controls: Impacts on Grid Performance" IEEE Power and Energy Society General Meeting, Jul. 2011.
8. X. Xi, H. Geng, and G. Yang, "Small signal stability of weak power system integrated with inertia tuned large scale wind farm," IEEE PES Innovative Smart Grid Technologies (ISGT), Kuala Lumpur, pp.514-518, 2014.
9. J. Ma, Y. Qiu, Y. Li, W. Zhang, Z. Song and J. S. Thorp, "Research on the impact of DFIG virtual inertia control on power system small-signal stability considering the phase-locked loop," IEEE Trans. Power Syst., to be published.
10. G.Tsourakis, B. M. Nomikos, and C. D. Vournas, "Contribution of doubly fed wind generators to oscillation damping", IEEE Trans. Energy Convers., vol. **24**, no. 3, pp. 783-791, Sept. 2009.
11. K. Clark, N. W. Miller, J. J. Sanchez-Gasca. “Modeling of GE wind turbine generators for grid studies”, version 4.5, (2010).